Aerodynamic Shape Optimization Using Automatic Adaptive Remeshing

G. Bugeda
E. Oñate
D. Joannas

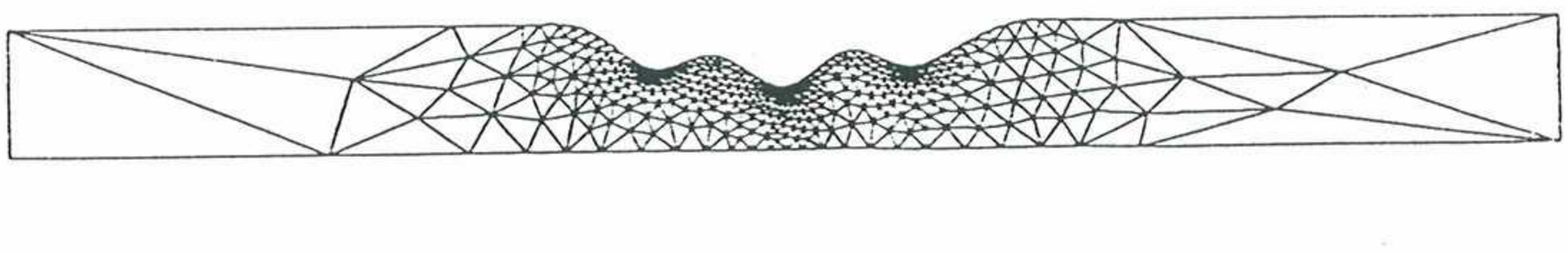

Publicación CIMNE Nº 29, February 1993

Aerodynamic Shape Optimization Using Automatic Adaptive Remeshing

G. Bugeda
E. Oñate
D. Joannas

Publicación CIMNE Nº 29, February 1993

Centro Internacional de Métodos Numéricos en Ingeniería
Gran Capitán s/n, 08034 Barcelona, España

AERODYNAMIC SHAPE OPTIMIZATION USING AUTOMATIC ADAPTIVE REMESHING

G. BUGEDA, E. OÑATE, D. JOANNAS

Escola Tècnica Superior d'Enginyers de Camins, Canals i Ports
Universitat Politècnica de Catalunya
Módulo C1; Campus Norte UPC; Gran Capitán s/n;08034 Barcelona;Spain

SUMMARY

This work presents a new methodology based on the use of adaptive mesh refinement (AMR) techniques in the context of shape optimization problems analyzed by the Finite Element Method. A suitable and very general technique for the parametrization of the optimization problem using B-splines to define the boundary is first presented. Then, mesh generation using the advancing front method, the estimation of error and the mesh refinement criterion are studied in the context of shape optimization problems. In particular, the sensitivities of the different ingredients ruling the problem (B-splines, finite element mesh, flow behaviour, and error estimator) are studied in detail. The sensitivities of the finite element mesh and the error estimator allow their projection from one design to the next, thus leading to an "a priori knowledge" of the error distribution on the new design without the need of any additional analysis. This information allows to build up a finite element mesh for the new design with an specified and controlled level of error. The robustness and reliability of the proposed methodology is checked out with some 2D application examples.

1. INTRODUCTION

From a mathematical point of view the treatment of an optimization or an inverse problem can be viewed as the minimization of a real function $f(\boldsymbol{x})$ depending on a set of variables ($\boldsymbol{x} = \{x_i\}\ ; i = 1, ..., n$). Each set defines a different design and the problem consists of finding those $\boldsymbol{x}$ values defining the best design.

The algorithms for the solution of the minimization problem are, typically, iterative and they involve the computation of the derivatives (sensitivities) of the objective function with respect to the design variables. Besides, in each step of the process, the computation of the f values and their sensitivities is needed. In many cases, as those considered in this work, the computations are performed via a finite element analysis which provides the aerodynamic response of each design, and a way to compute the corresponding sensitivities. The definition of each design in terms of the $\boldsymbol{x}$ variables is called the "parametrization" of the optimum design problem.

The author's contribution to the EUROPT I [4,5] project has been the development of a new methodology for optimization and inverse aerodynamic problems including an adaptive remeshing procedure. The main characteristics of this methodology are:

- The control of the error involved in the numerical solution of the flow equations for each design using an error estimator. This is used for the generation of a new mesh for each design.

- The use of first and second order *exact* sensitivity analysis of all the magnitudes involved in the process, including the coordinates of the mesh, the velocities, the objective function and the error estimator.
- The *projection* of the information obtained with one design to the next one, using the mentioned sensitivity analysis. This projection is used to define the characteristics of the mesh which will ensure good quality results for the next design.
- The parametrization of the problem using B-splines. The coordinates of the points used to define a B-spline are used as design variables.

The proposed methodology has been implemented in a computer code using an incompressible potential flow model. The code has been tested by solving different 2D applications like the workshop test cases defined for the EUROPT I project [20].

2. THE PROPOSED METHODOLOGY

A general scheme of the proposed methodology is shown in Figure 1. It consists of a series of modules each one corresponding to a specific task. In the next sections some of these modules are discussed in detail.

For each design it is necessary to compute the sensitivities of the objective function. The sensitivity analysis for the whole problem is performed step by step following the same path as the flow analysis. This path indicates the dependence of each quantity used in the analysis with respect to the rest of the quantities previously employed. For example, the expression of the finite element matrix depends on the nodal coordinates, so that, following the chain rule for derivatives, the finite element matrix sensitivities can be expressed in terms of the nodal coordinates sensitivities. Thus, it is necessary to compute these sensitivities (mesh sensitivities) prior to that of the finite element matrix sensitivities.

First-order and second-order sensitivity analyses have been used in the implementation of the proposed methodology. The sensitivity analysis provides directional derivatives of any quantity. In the next paragraphs the $\boldsymbol{s}$ will denote a unit vector in the design variables space ($\boldsymbol{x} = \{x_1, x_2, ..., x_i, ..., x_n\}$), and derivatives will be computed in the $\boldsymbol{s}$ direction. For instance, to obtain the sensitivities with respect to a specific design variable x_i, $\boldsymbol{s}$ has to be the unit vector corresponding to the x_i direction (i.e. $\boldsymbol{s} = \{0, 0, ..., 1, ..., 0\}$).

The sensitivities of any quantity will be used to project its value from one design to the next one when the design variables are modified. For example, let us assume that $f(\boldsymbol{x}^k)$ is the objective function value at the k-th iteration of the optimization process. If the design variables are modified in the form $\boldsymbol{x}^{k+1} = \boldsymbol{x}^k + \theta^k \boldsymbol{s}^k$, the value of the objective function can be projected to the next design by means of a standard Taylor expansion:

$$f(\boldsymbol{x}^{k+1}) = f(\boldsymbol{x}^k + \theta \boldsymbol{s}^k) \approx f(\boldsymbol{x}^k) + \theta^k \frac{\partial f}{\partial \boldsymbol{s}} + \frac{1}{2}\theta^{k\,2} \frac{\partial^2 f}{\partial \boldsymbol{s}^2} \tag{1}$$

The same applies to any other magnitude to be projected.

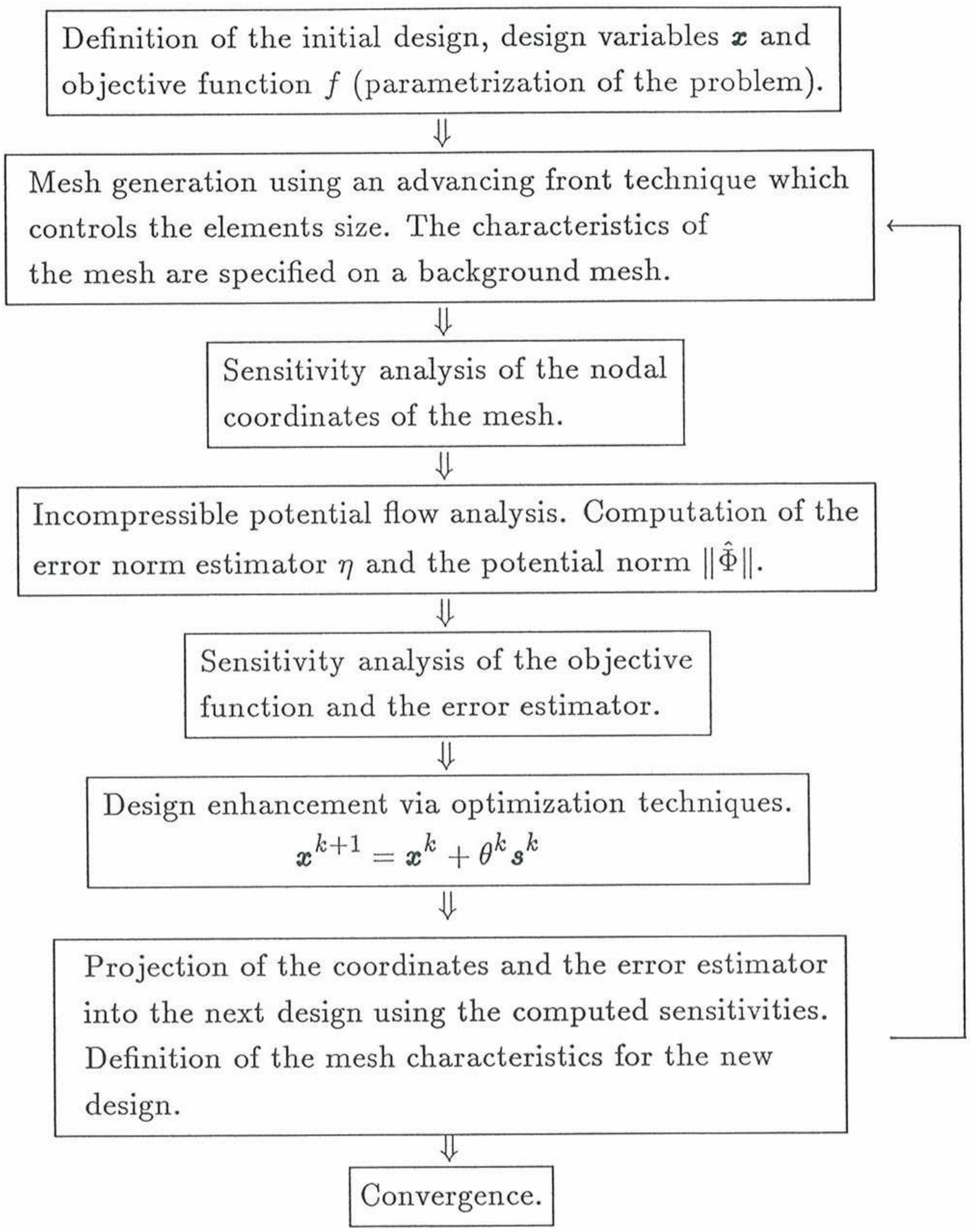

FIGURE 1. General scheme of the proposed methodology.

3. PARAMETRIZATION OF THE PROBLEM

The description of each design geometry is done by using "definition points" which specify some interpolation curves. The curves used here are parametric B-splines. The general expression of a closed B-spline for q points is [1,6]:

$$\boldsymbol{r}(t) = \sum_{l=0}^{q} \boldsymbol{r}_l N_{4,l+1}(t) \tag{2}$$

where $\boldsymbol{r}(t)$ is the position vector depending on a parametric variable t. The coordinates of the definition points are recovered using $t = 0, 1, 2, ...$ The curve is expressed as a linear combination of $q + 1$ normalized fourth order (cubic) B-splines [1,6]. The $\boldsymbol{r}_l$ coefficients are the coordinates of the so called polygon definition points [1,6] and they

are found by using the coordinates of the definition points. The degree of continuity of a cubic B-spline is C^2. By using eq. (2) the coordinates of the definition points and some additional conditions about slopes and curvatures the following equations system can be found:

$$\boldsymbol{V} = \boldsymbol{N}\boldsymbol{R} \tag{3}$$

where $\boldsymbol{V}$ is a vector containing the imposed conditions at the definition points, $\boldsymbol{N}$ is a matrix containing some terms corresponding to the values of the polynomials that define each B-spline, and the $\boldsymbol{R}$ vector contains the coefficients $\boldsymbol{r}_i$ to be computed. Details of this process can be found in [1,6].

The first and second order sensitivities of $\boldsymbol{R}$ along a direction $\boldsymbol{s}$ in the design variable space are given by:

$$\frac{\partial \boldsymbol{R}}{\partial \boldsymbol{s}} = \boldsymbol{N}^{-1}\left(\frac{\partial \boldsymbol{V}}{\partial \boldsymbol{s}} - \frac{\partial \boldsymbol{N}}{\partial \boldsymbol{s}}\boldsymbol{R}\right) \quad , \quad \frac{\partial^2 \boldsymbol{R}}{\partial \boldsymbol{s}^2} = \boldsymbol{N}^{-1}\left(\frac{\partial^2 \boldsymbol{V}}{\partial \boldsymbol{s}^2} - \frac{\partial^2 \boldsymbol{N}}{\partial \boldsymbol{s}^2}\boldsymbol{R} - 2\frac{\partial \boldsymbol{N}}{\partial \boldsymbol{s}}\frac{\partial \boldsymbol{R}}{\partial \boldsymbol{s}}\right) \tag{4}$$

The derivatives of $\boldsymbol{V}$ with respect the coordinates of the definition points chosen as design variables can be very easily computed. Vectors $\frac{\partial \boldsymbol{R}}{\partial \boldsymbol{s}}$ and $\frac{\partial^2 \boldsymbol{R}}{\partial \boldsymbol{s}^2}$ will contain the terms $\frac{\partial \boldsymbol{r}_i}{\partial \boldsymbol{s}}$ and $\frac{\partial^2 \boldsymbol{r}_i}{\partial \boldsymbol{s}^2}$, respectively [1].

Finally, the sensitivities of the coordinates of any point on the interpolation curve corresponding to $t = constant$ are obtained by:

$$\frac{\partial \boldsymbol{r}(t)}{\partial \boldsymbol{s}} = \sum_{i=0}^{q} \frac{\partial \boldsymbol{r}_i}{\partial \boldsymbol{s}} N_{4,i+1}(t) \quad , \quad \frac{\partial^2 \boldsymbol{r}(t)}{\partial \boldsymbol{s}^2} = \sum_{i=0}^{q} \frac{\partial^2 \boldsymbol{r}_i}{\partial \boldsymbol{s}^2} N_{4,i+1}(t) \tag{5}$$

4. MESH GENERATION AND SENSITIVITY ANALYSIS

The chosen algorithm to generate the mesh is the well known advancing front method [12,13]. This technique is ideal to generate non structured triangular meshes.

The characteristics of the desired mesh are specified via a background mesh over which nodal values of the size parameters δ are defined and interpolated using the shape functions. For the first design the background mesh has to be defined by hand. For subsequent designs the background mesh will coincide with the mesh projected into this design from the previous one. This projection will be described later.

Once the sensitivities of the coordinates of each boundary node are known, it is also possible to compute the sensitivities of the coordinates of each internal nodal point (mesh sensitivities). These sensitivities are used to asses how the mesh moves when the design variables change.

For non-structured meshes the sensitivity analysis can be obtained by studying the variations of the mesh due to changes in the design variables. There are many different ways to define the movement of the mesh in terms of the design variables. It is possible to consider a simple analogous elastic medium defining the mesh movement. This is the case of the "spring analogy" where each element side is regarded as a spring

connecting two nodes. The force produced by each spring is proportional to its length. The solution of the equilibrium problem in the spring analogy is simple but expensive and it involves to solve a linear system of equations with two of degrees of freedom for each node.

The spring analogy problem can be solved iteratively using a Laplacian smoothing, as it has been done in the present work. This technique is frequently used to improve the quality of non-structured meshes. It consists on the iterative modification of the nodal coordinates of each interior node by placing it at the center of gravity of the adjacent nodes. For each iteration the expression of the new position vector of each node $\boldsymbol{r}_i$ is given by:

$$\boldsymbol{r}_i = \frac{\sum_{j=1}^{m_i} \boldsymbol{r}_j}{m_i} \tag{6}$$

where $\boldsymbol{r}_j$ are the position vectors of the m_i nodes connected with the i-th node.

The solution of the spring analogy problem with a prescribed error tolerance requires to check the solution after each smoothing cycle. Taking into account that the described iterative process is only a way to obtain mesh sensitivities, rather than the solution of the equilibrium problem itself, rigorous convergence conditions are not needed. For this reason the number of smoothing cycles to be applied can be fixed a priori. In the examples presented below we have checked that 50 iterations are enough to ensure a good quality of the results.

The first-order and higher mesh sensitivity analysis in any direction of the design variables space, $\boldsymbol{s}$, are obtained by differentiating eq. (6) with respect to $\boldsymbol{s}$ for each cycle, i.e.

$$\frac{\partial \boldsymbol{r}_i}{\partial \boldsymbol{s}} = \frac{\sum_{j=1}^{m_i} \frac{\partial \boldsymbol{r}_j}{\partial \boldsymbol{s}}}{m_i} \quad , \quad \frac{\partial^2 \boldsymbol{r}_i}{\partial \boldsymbol{s}^2} = \frac{\sum_{j}^{m_i} \frac{\partial^2 \boldsymbol{r}_j}{\partial \boldsymbol{s}^2}}{m_i} \tag{7}$$

5. FLOW ANALYSIS AND ERROR ESTIMATION

The basic equations for the analysis of the flow around a profile using an incompressible potential model with lifting involve a "continuous" potential Φ_0 and a "non-continuous" potential Φ_1 which are combined in order to accomplish the Kutta-Joukowski condition [14].

Let us consider a domain Ω where the flow problem is defined. A cut Σ between the trailing edge Te and the boundary of Ω is defined (see Figure 2). The upper and lower sides of the cut are noted Σ^+ and Σ^-, respectively.

The corresponding equations for the "continuous" and the "non continuous" potentials are [14]:

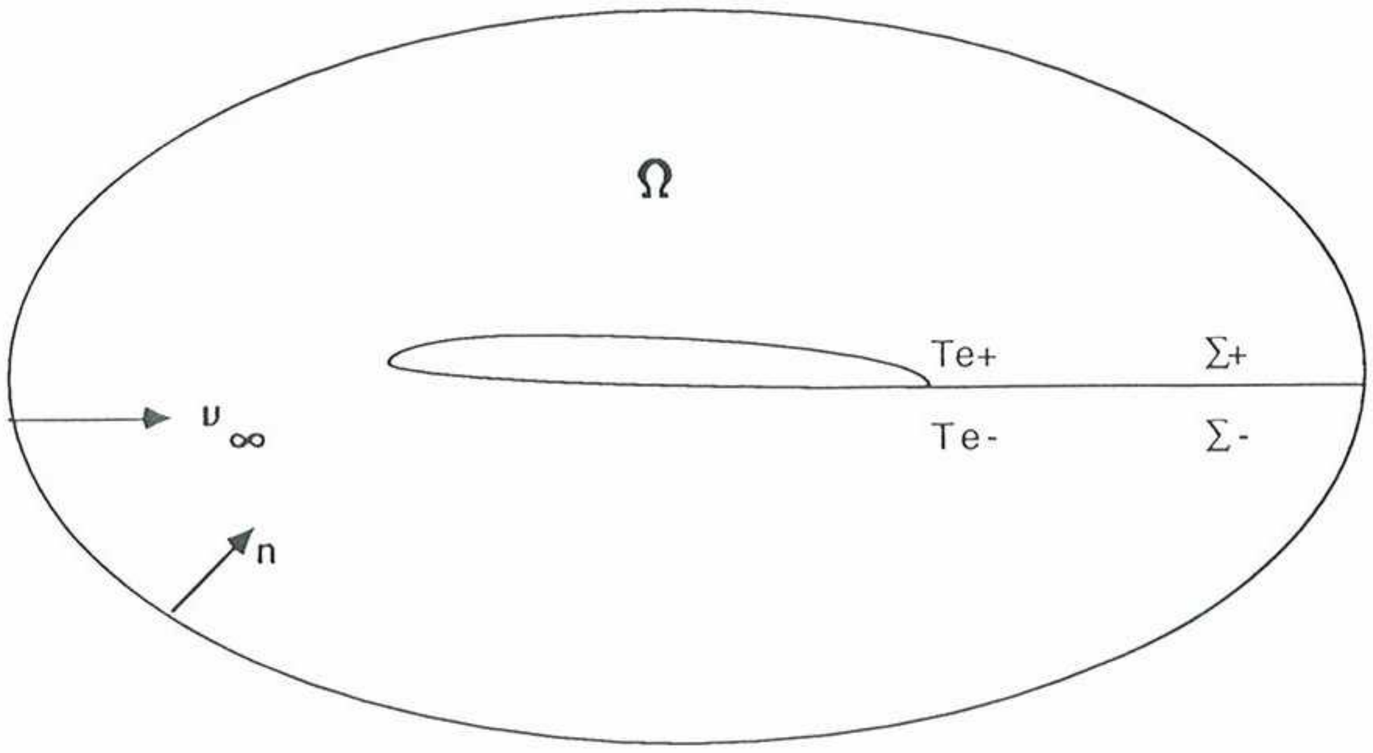

Figure 2. Analysis domain for the potential flow with lifting problem.

$$\begin{cases} \Delta\Phi_0 = 0 \\ \Phi_0|_{\Sigma^+} - \Phi_0|_{\Sigma^-} = 0 \\ \frac{\partial\Phi_0}{\partial n^+}|_{\Sigma^+} + \frac{\partial\Phi_0}{\partial n^-}|_{\Sigma^-} = 0 \\ \frac{\partial\Phi_0}{\partial n}|_{\partial\Omega} = \boldsymbol{v}_\infty \boldsymbol{n} \\ \Phi_0(Te^-) = 0 \end{cases} \qquad \begin{cases} \Delta\Phi_1 = 0 \\ \Phi_1|_{\Sigma^+} - \Phi_1|_{\Sigma^-} = 1 \\ \frac{\partial\Phi_1}{\partial n^+}|_{\Sigma^+} + \frac{\partial\Phi_1}{\partial n^-}|_{\Sigma^-} = 0 \\ \frac{\partial\Phi_1}{\partial n}|_{\partial\Omega} = 0 \\ \Phi_0(Te^-) = 0 \end{cases} \tag{8}$$

Both potentials are combined to get the final solution $\Phi = \Phi_0 + \lambda\Phi_1$ where λ is obtained from the Kutta-Joukowski condition [14] which ensures the continuity of the upper and lower velocities at the trailing edge.

The velocities at each point are obtained from the gradient of the potentials $\boldsymbol{v} = \nabla\Phi = \nabla\Phi_0 + \lambda\nabla\Phi_1$.

If more than one airfoil is involved a non continuous potential is defined for each geometry and the Kutta-Joukowski condition is applied to each trailing edge.

The discretization of eqs. (8) for each potential Φ using a finite element approximation, i.e. $\Phi \approx \hat{\Phi} = \sum_i N_i a_i = \boldsymbol{N}\boldsymbol{a}$, leads to a linear system of equations, i.e.

$$\boldsymbol{K}\boldsymbol{a} = \boldsymbol{f} \quad with \quad \begin{cases} \boldsymbol{K} = \sum_e \boldsymbol{K}_e \\ \boldsymbol{K}_e = \int_{\Omega_e} \boldsymbol{B}^T \boldsymbol{B} d\Omega \\ \boldsymbol{f} = \int_{\Gamma_e} \boldsymbol{N}\boldsymbol{v}^T \boldsymbol{n} d\Gamma \end{cases} \tag{9}$$

Matrix $\boldsymbol{B}$ contains the cartesian derivatives of the shape functions N_i and it can be used to obtain the velocities corresponding to the approximated potential $\hat{\boldsymbol{v}} = \boldsymbol{B}\Phi$.

For incompressible potential problems the "energy" of the exact solution can be defined as:

$$\|U\| = [\int_\Omega \boldsymbol{v}^T \boldsymbol{v} d\Omega]^{1/2} \tag{10}$$

The error of this "energy" can be estimated using the popular error estimator developed by Zienkiewicz and Zhu [15–19] for structural problems. The extension to potential flow problems requires the definition of the following error norm [3,4]:

$$\|e\| = [\int_\Omega [\boldsymbol{v} - \hat{\boldsymbol{v}}]^T [\boldsymbol{v} - \hat{\boldsymbol{v}}] d\Omega]^{1/2} \tag{11}$$

where $\boldsymbol{v}$ are the "exact" velocities, $\hat{\boldsymbol{v}}$ are the velocities obtained from the finite element solution and Ω is the flow analysis domain.

Since the exact velocities are usually not known they are approximated by $\boldsymbol{v} \simeq \boldsymbol{v}^* = \boldsymbol{N}\bar{\boldsymbol{v}}^*$ where $\bar{\boldsymbol{v}}^*$ are nodal values obtained by simple nodal averaging of the finite element values, local or global least squares smoothing, or other adequate projection methods [15–19]. A simple approach is to use a global nodal smoothing with a "mass" matrix giving the nodal smoothed values, $\bar{\boldsymbol{v}}^*$, as

$$\bar{\boldsymbol{v}}^* = \boldsymbol{M}^{-1} \int_\Omega \boldsymbol{N}_v \hat{\boldsymbol{v}} d\Omega \tag{12}$$

where $\boldsymbol{N}_v$ are the chosen velocity interpolating functions giving a smooth nodal velocity field [15–19] and $M_{ij} = \int_\Omega N_{v_i} N_{v_j} d\Omega$. Eq. (12) can be obviously applied to solve independently for each individual velocity component.

The "energy" of the exact solution is estimated as

$$\|U\| \approx [\int_\Omega \boldsymbol{v}^{*T} \boldsymbol{v}^* d\Omega + \int_\Omega [\boldsymbol{v}^* - \hat{\boldsymbol{v}}]^T [\boldsymbol{v}^* - \hat{\boldsymbol{v}}] d\Omega]^{1/2} \tag{13}$$

Both $\|e\|^2$ and $\|U\|^2$ can be evaluated as sum of their respective element contributions.

6. SENSITIVITY ANALYSIS OF THE OBJECTIVE FUNCTION AND THE ERROR ESTIMATOR

The objective function will be normally expressed in terms of the velocities, pressures, etc. obtained from the flow model. To compute the sensitivity of the objective function it is necessary to evaluate the sensitivity of all the magnitudes involved in the flow analysis.

The exact sensitivity analysis of all the integral expressions involved in the finite element discretization of the incompressible potential flow model can be obtained by direct derivation of eqs. (9). This provides the sensitivities of all magnitudes in terms of the mesh sensitivities previously obtained. Details of this process are described in references [1,7,8]. The corresponding expressions can be separately applied to each potential (Φ_0, Φ_1,...).

For a single airfoil, the sensitivity analysis of the total potential $\hat{\Phi} = \hat{\Phi}_0 + \lambda \hat{\Phi}_1$ involves a combination of the sensitivities of Φ_0, Φ_1 and λ.

$$\frac{\partial \hat{\Phi}}{\partial \boldsymbol{s}} = \frac{\partial \hat{\Phi}_1}{\partial \boldsymbol{s}} + \lambda \frac{\partial \hat{\Phi}_2}{\partial \boldsymbol{s}} + \frac{\partial \lambda}{\partial \boldsymbol{s}} \hat{\Phi}_2 \quad , \quad \frac{\partial^2 \hat{\Phi}}{\partial \boldsymbol{s}^2} = \frac{\partial^2 \hat{\Phi}_1}{\partial \boldsymbol{s}^2} + \lambda \frac{\partial^2 \hat{\Phi}_2}{\partial \boldsymbol{s}^2} + 2 \frac{\partial \lambda}{\partial \boldsymbol{s}} \frac{\partial^2 \hat{\Phi}_2}{\partial \boldsymbol{s}^2} + \frac{\partial^2 \lambda}{\partial \boldsymbol{s}^2} \hat{\Phi}_2 \tag{14}$$

The terms $\partial\lambda/\partial \boldsymbol{s}$ and $\partial^2\lambda/\partial \boldsymbol{s}^2$ can be obtained by direct derivation of the Kutta-Joukowski condition.

The same operation can be performed to compute the sensitivities of the velocities at the integration points ($\hat{\boldsymbol{v}}$) and the nodal points ($\bar{\boldsymbol{v}}^*$) i.e.

$$\frac{\partial \hat{\boldsymbol{v}}}{\partial \boldsymbol{s}} = \frac{\partial \hat{\boldsymbol{v}_1}}{\partial \boldsymbol{s}} + \lambda \frac{\partial \hat{\boldsymbol{v}_2}}{\partial \boldsymbol{s}} + \frac{\partial \lambda}{\partial \boldsymbol{s}} \hat{\boldsymbol{v}_2} \quad , \quad \frac{\partial^2 \hat{\boldsymbol{v}}}{\partial \boldsymbol{s}^2} = \frac{\partial^2 \hat{\boldsymbol{v}_1}}{\partial \boldsymbol{s}^2} + \lambda \frac{\partial^2 \hat{\boldsymbol{v}_2}}{\partial \boldsymbol{s}^2} + 2 \frac{\partial \lambda}{\partial \boldsymbol{s}} \frac{\partial^2 \hat{\boldsymbol{v}_2}}{\partial \boldsymbol{s}^2} + \frac{\partial^2 \lambda}{\partial \boldsymbol{s}^2} \hat{\boldsymbol{v}_2} \quad (15)$$

$$\frac{\partial \bar{\boldsymbol{v}}^*}{\partial \boldsymbol{s}} = \frac{\partial \bar{\boldsymbol{v}}^*{}_1}{\partial \boldsymbol{s}} + \lambda \frac{\partial \bar{\boldsymbol{v}}^*{}_2}{\partial \boldsymbol{s}} + \frac{\partial \lambda}{\partial \boldsymbol{s}} \bar{\boldsymbol{v}}^*{}_2 \quad , \quad \frac{\partial^2 \bar{\boldsymbol{v}}^*}{\partial \boldsymbol{s}^2} = \frac{\partial^2 \bar{\boldsymbol{v}}^*{}_1}{\partial \boldsymbol{s}^2} + \lambda \frac{\partial^2 \bar{\boldsymbol{v}}^*{}_2}{\partial \boldsymbol{s}^2} + 2 \frac{\partial \lambda}{\partial \boldsymbol{s}} \frac{\partial^2 \bar{\boldsymbol{v}}^*{}_2}{\partial \boldsymbol{s}^2} + \frac{\partial^2 \lambda}{\partial \boldsymbol{s}^2} \bar{\boldsymbol{v}}^*{}_2 \quad (16)$$

Very similar equations to (14), (15) and (16) hold for cases with more than one airfoil. Here there are as many λ parameters as different components where the Kutta-Joukowski condition is imposed. These parameters are obtained by solving a non linear system of equations, each one corresponding to the Kutta-Joukowski condition applied over one airfoil. To obtain the sensitivities of the λ parameters it is necessary to derivate this system of equations with respect to the velocities at the trailing edge of each airfoil.

The computation of C_p and its sensitivities in terms of the velocities for the case of an incompressible flow is trivial using the expression:

$$C_p = 1 - \left(\frac{|\boldsymbol{v}|}{|\boldsymbol{v}_\infty|} \right)^2 \quad (17)$$

The sensitivities of the objective function can be obtained by its direct derivation with respect to the design variables. These sensitivities will be expressed in terms of the sensitivities of the nodal velocities.

The sensitivities of the error estimator and the "energy" of the solution can be obtained in terms of the sensitivities of the velocities by appropriate derivation of the integral expressions (11) and (13) [1,7,8].

7. DESIGN IMPROVEMENT

The objective function sensitivities are used to get improved values of the design variables by means of a minimization method. Depending on the optimization algorithm it may be necessary to use second order sensitivities. The design variables corresponding to the improved design will usually be found as:

$$\boldsymbol{x}^{k+1} = \boldsymbol{x}^k + \theta \boldsymbol{s}^k \quad (18)$$

where θ is an advance parameter.

The direction of change $\boldsymbol{s}^k$ has been obtained here using a BFGS Quasi-Newton method which only requires first order sensitivities of the objective function. The value of θ is obtained by a directional second order sensitivity analysis in the $\boldsymbol{s}^k$ direction. The objective function f can be approximated along this direction using a second order Taylor expansion similar to eq. (1) which minimization provides the value of θ. Details of this algorithm can be found in [7].

8. PROJECTION TO THE NEXT DESIGN AND DEFINITION OF THE NEW MESH

Once the new design has been defined the new values of the error estimator, the "energy" and the coordinates of the mesh can be projected from the previous solution as:

$$(x,y)^{k+1} = (x,y)^k + \theta\Big(\frac{\partial x}{\partial s},\frac{\partial y}{\partial s}\Big) + \frac{1}{2}\theta^2\Big(\frac{\partial^2 x}{\partial s^2},\frac{\partial^2 y}{\partial s^2}\Big) \tag{19}$$

$$\|e\|^{2^{k+1}} = \|e\|^{2^k} + \theta\frac{\partial\|e\|^2}{\partial s} + \frac{1}{2}\theta^2\frac{\partial^2\|e\|^2}{\partial s^2} \tag{20}$$

$$\|U\|^{2^{k+1}} = \|U\|^{2^k} + \theta\frac{\partial\|U\|^2}{s} + \frac{1}{2}\theta^2\frac{\partial^2\|U\|^2}{\partial s^2} \tag{21}$$

These projections provide a good approximation of each of above values for the next design previously to any new computation. In fact, the projected values provide the necessary information to perform a remeshing over the next design, even before any new computation is performed. In that sense, we have converted an error estimator computed "a posteriori" into an "a priori" error estimator.

This projection is very important because it allows the quality control of the meshes for each design without any new remeshing. Only one initial mesh is generated and this is used over each design. Thus, the extra cost involved in the control of the mesh quality is very cheap.

The projected values are used to create the background mesh information needed to generate the first mesh for the new design. This operation closes the iterative process which will lead to the 'enhanced" optimum design after convergence.

For the complete definition of the characteristics of a new mesh in the remeshing procedure it is necessary to use a mesh optimality criterion. In this work a mesh is considered as optimal when the error density is equally distributed across the volume, i.e. when $\frac{\|e\|_e^2}{\Omega_e} = \frac{\|e\|^2}{\Omega}$ is satisfied. The justification of this optimality criterion can be found in [9–11].

The combination of the optimality criterion and the error estimation allows to define the new element sizes. Previously, it is necessary to define the limit of the allowable global error percentage γ as:

$$\gamma = 100\frac{\|e\|}{\|\Phi\|} \approx 100\frac{\|e\|}{\sqrt{\|e\|^2 + \|\hat{\Phi}\|^2}} \tag{22}$$

The desired error level for each element is:

$$\|e\|_e^d = \frac{\gamma}{100}\sqrt{(\|\hat{\Phi}\|^2 + \|e\|^2)\frac{\Omega_e}{\Omega}} \tag{23}$$

The new element sizes $\bar{h}_e$ can be computed in terms of the old ones h_e using the expression:

$$h = \frac{h_e}{\xi_e^{1/p}} \tag{24}$$

where $\xi_e = \frac{\|e\|_e}{\|e\|_e^d}$ and p is the order of the shape function polynomials. For further details see [1−3,9−11].

9. APPLICATION EXAMPLES

The methodology developed in this work has been implemented in a computer code in order to check its reliability. Test cases T1, T2 and T4 of the workshop on Optimum Design in Aerodynamics held in Barcelona on June 1992 [20] have been solved and its corresponding results are presented below. The results corresponding to a problem of a two components airfoil are also presented here below.

9.1 T1 workshop test case

This test case consists in recovering a nozzle starting from a straight line. The target shape is defined by the following sine curve:

$$y(x) = 0.375 + 0.125 sin(\pi(x - 1.500)) \tag{25}$$

The target pressure coefficient C_p^{target} has been obtained using the defined target shape and computing it with a finite element code using the incompressible potential model previously defined and adaptive remeshing. Quadratic triangular elements (P2) have been used for the analysis. The maximum error γ has been limited to 0.1%.

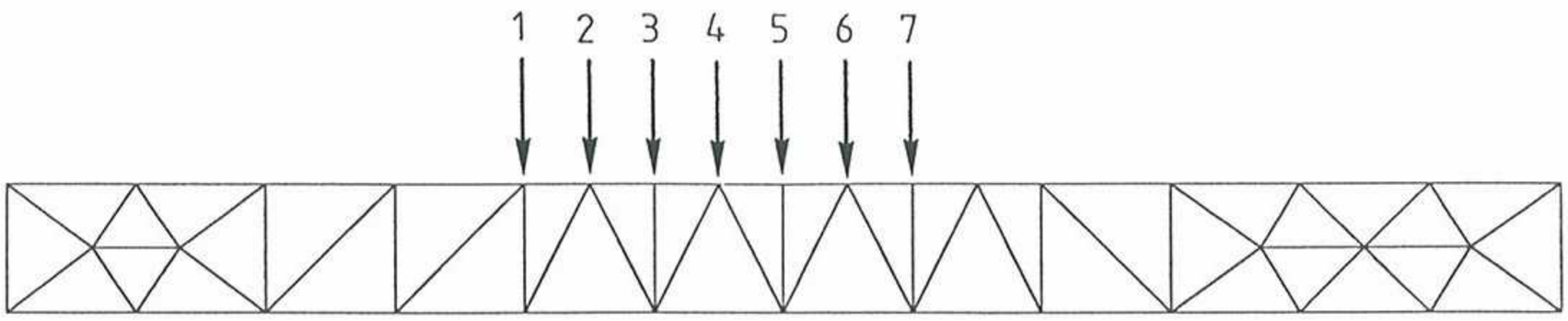

Figure 3. Initial shape, initial mesh and definition of the design variables.

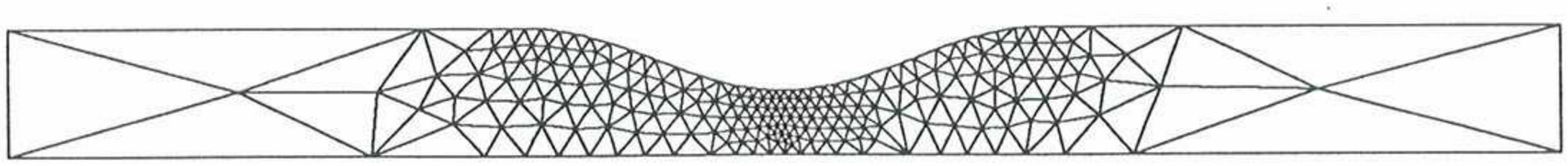

Figure 4. Final shape and final mesh.

The inverse problem has been solved using a minimization approach. The cost functional to be minimized has been defined as:

$$f = \int_0^2 (C_p(x) - C_p^{target})^2 dx \tag{26}$$

The geometry of each design has been defined using 7 design variables. This variables are the y coordinates of 7 points which are used to interpolate a B-spline along the top line. Figure 3 shows the initial shape, the position of the 7 design variables and the finite element mesh used for the analysis of initial design.

The iterative process has converged after 33 iterations. The final shape and the corresponding final mesh can be observed in Figure 4. Note the "quality" of the refinement automatically obtained in the zones where the solution error is greated. The whole problem has taken around 18 minutes of CPU running on a Personal Iris 35TG workstation.

The evolution of the normalized cost functional f during the process can be seen in Figure 5. Note that only one cost evaluation for each iteration is performed in the proposed methodology. Figure 6 shows the evolution of the normalized L2 norm of the cost functional gradient during the iterative process. Figure 7 shows the evolution of the normalized L2 difference norm between the solution and the design profiles. Figure 8 shows the evolution of the global percentage of error during the minimization process.

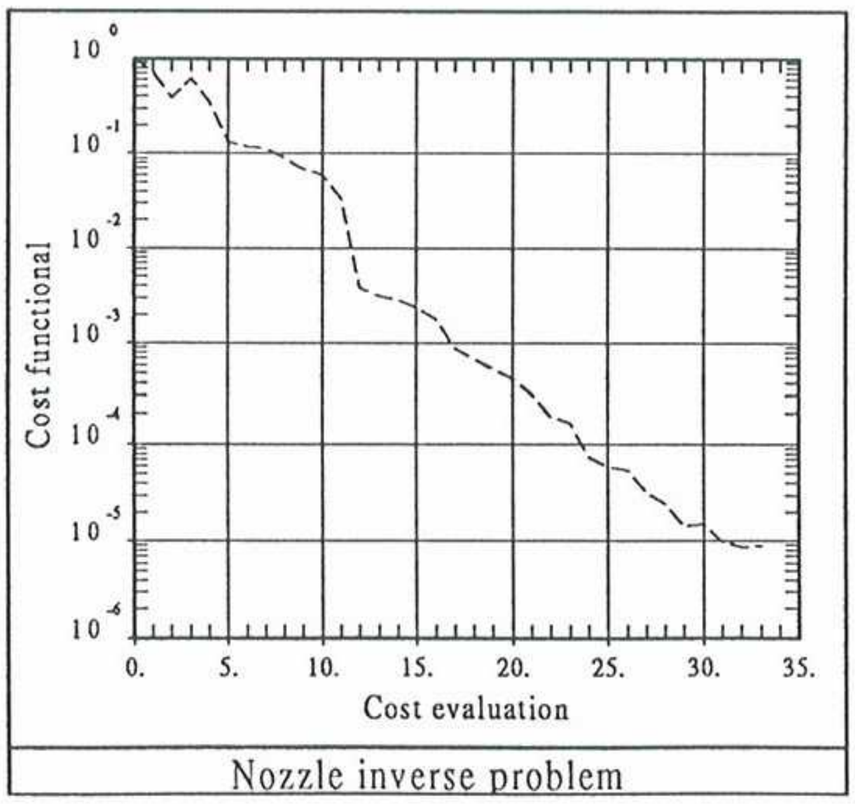

Figure 5. Evolution of the normalized cost functional during the iterative process.

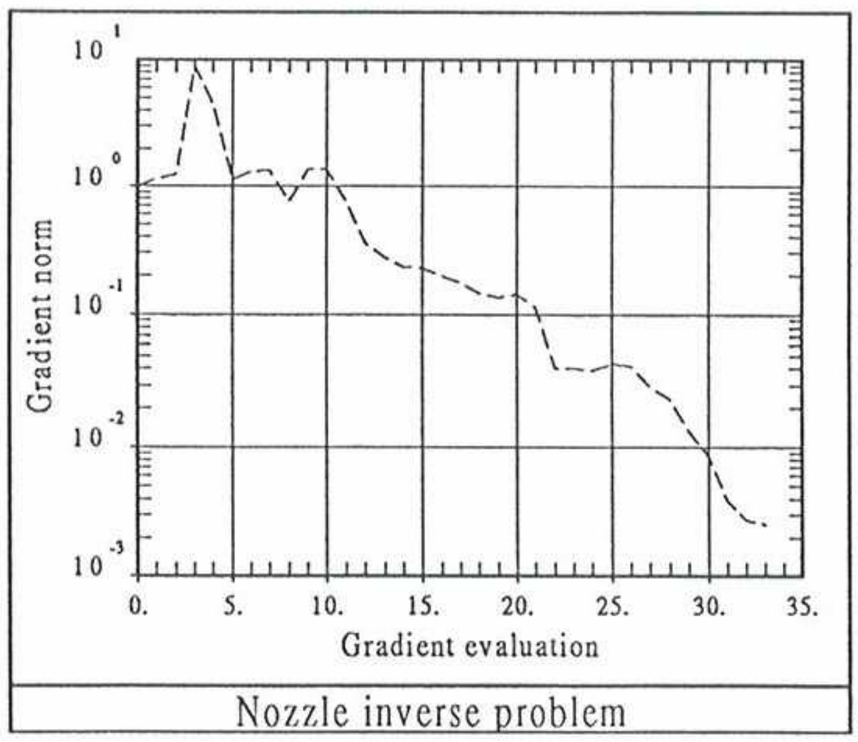

Figure 6. Evolution of the normalized L2 norm of the gradient of the cost functional.

Figures 5,6 and 7 show the fast convergence of the minimization process. The cost functional has been reduced 5 orders of magnitude in only 33 iterations. The norm of the objective function gradient has been reduced 4 orders of magnitude and the L2 difference norm has been reduced 3 orders of magnitude.

The global level of the error involved in the finite element computations has been fully controlled. After the seventh iteration it has been kept below the 0.1% limit imposed at the onset.

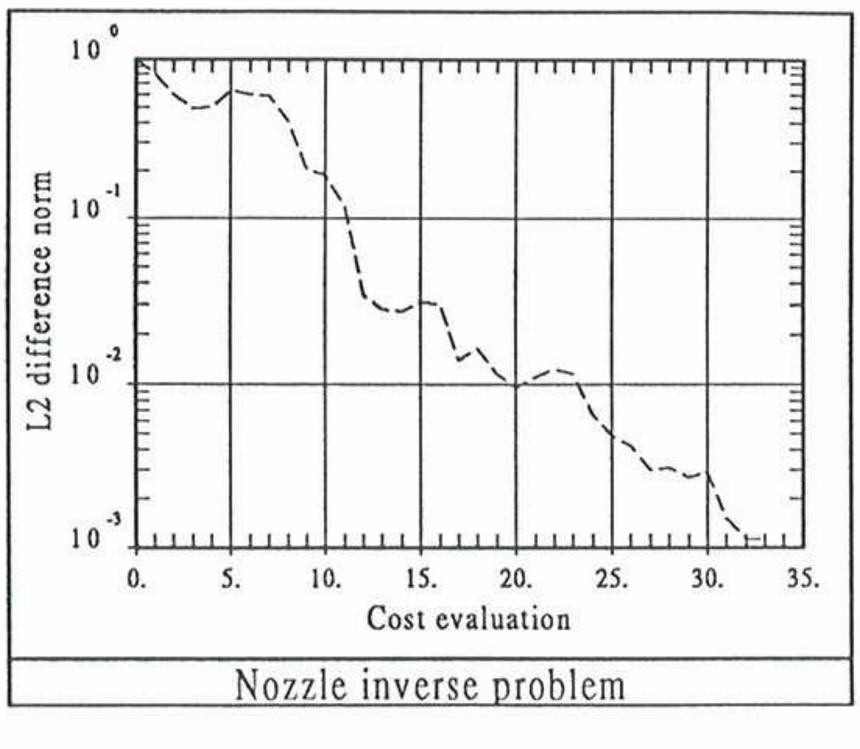

Figure 7. Evolution of the normalized L2 difference norm between the solution profile and the design profile.

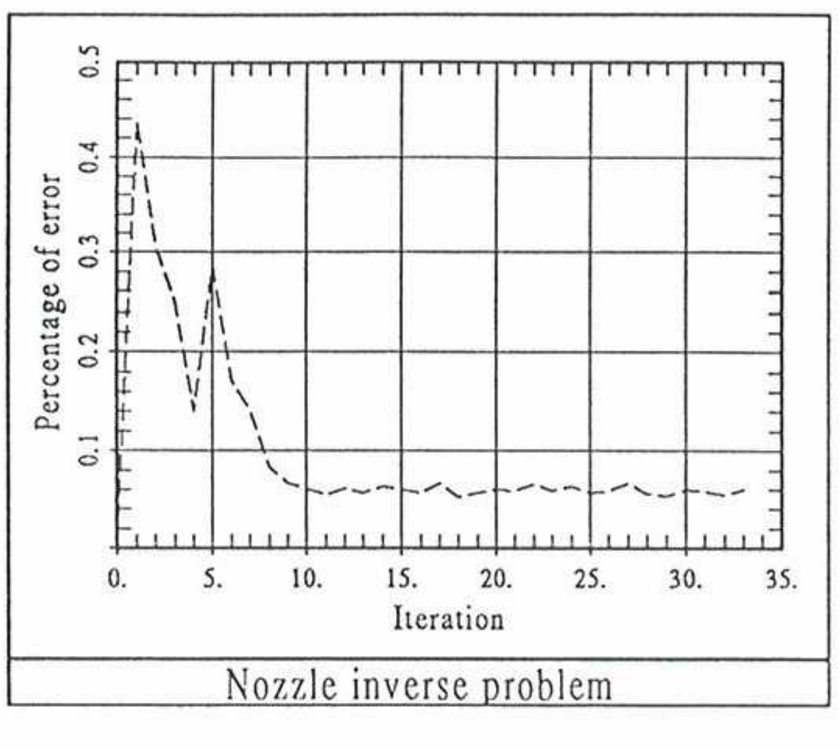

Figure 8. Evolution of the percentage of error.

9.2 T2 workshop test case

The T2 workshop test case consists in finding the shape which minimizes a cost function defined by the following integral expression over the bottom line of the nozzle:

$$\boldsymbol{f} = \int_0^2 \left| \frac{\partial p}{\partial x} \right|_{y=0}^{\alpha} dx, \qquad \alpha = 2 \;\; or \;\; 4 \tag{27}$$

with the constraint $y(1) = 0.25$

The geometry of each design has been defined using 6 design variables. These variables are the y coordinates of 6 points which are used to interpolate a B-spline along the top line. Figure 9 shows the initial shape, the position of the 6 design variables and the finite element mesh used for the initial design. This initial design is the target design defined for the T1 test case. The constraint $y(1) = 0.25$ is automatically achieved because the coordinates of the corresponding point are fixed. The maximum global error has been limited to 0.1% of the total potential norm.

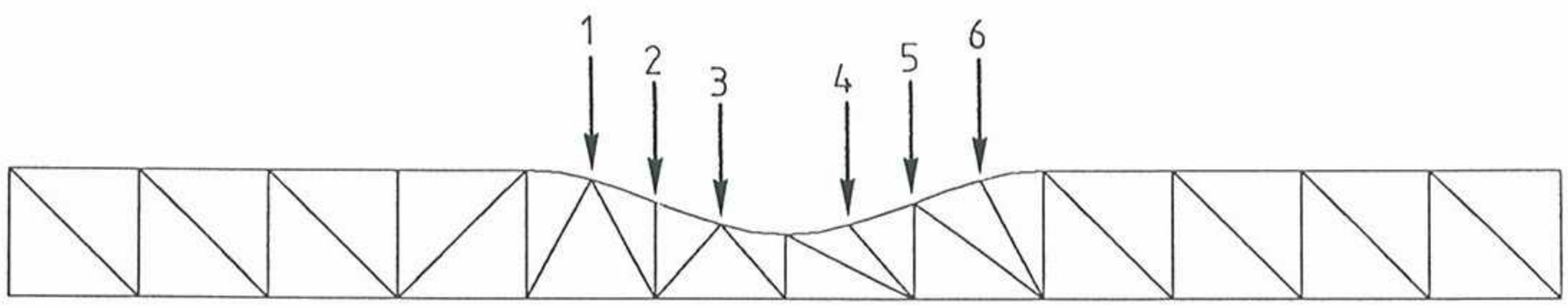

Figure 9. Initial shape, initial mesh and definition of the design variables.

This problem has been solved using $\alpha = 2$ (case 1) and $\alpha = 4$ (case 2) in both cases a strange solution has been obtained.

The final shape and the final mesh for case 1 can be observed in Figure 10. This shape has been obtained after 40 iterations. At this stage the process is not converged because the height of the waves seems to grow indefinitely. On the other hand, the value of the cost function remains almost constant during the last 20 iterations.

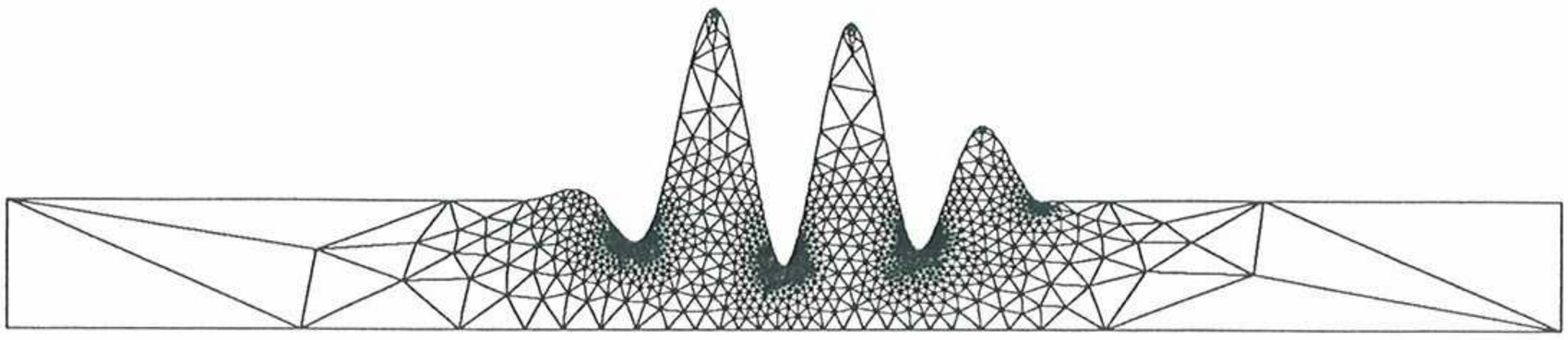

Figure 10. Final shape and final mesh for case 1.

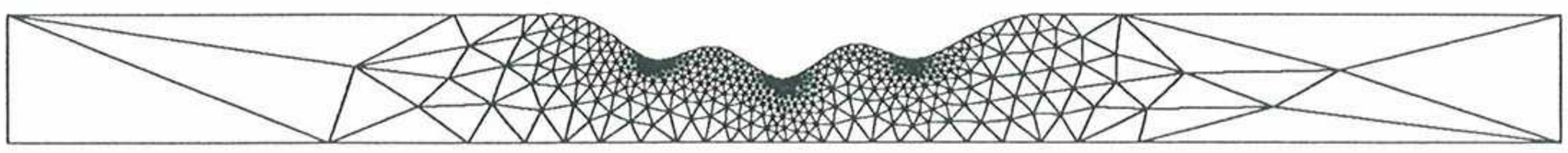

Figure 11. Final shape and final mesh for case 2.

The final shape and the final mesh for case 2 ($\alpha = 4$) can be seen in Figure 11. In this case the situation is very similar to case 1 but the formed waves are smaller.

After some study of the results obtained for cases 1 and 2 a different cost function has been defined. This new cost function has the same expression than the initial one but the integral expression is extended over the top line of the nozzle, i.e.

$$\boldsymbol{f} = \int_0^2 |\frac{\partial p}{\partial x}|^\alpha|_{y=y_{design}(x)} dx, \qquad \alpha = 2 \quad or \quad 4 \tag{28}$$

The final shape for this last case (case 3) can be observed in Figure 12.

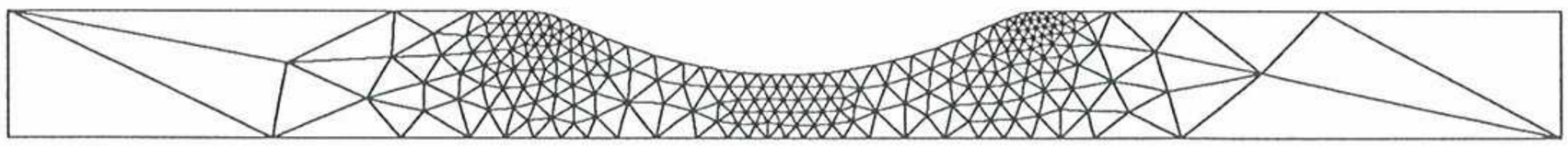

Figure 12. Final shape and final mesh for case 3.

The iterative process has now converged after 24 iterations. The whole problem has taken around 10 minutes of CPU on a Personal Iris 35TG workstation.

Figure 13 shows the evolution of the normalized cost functional during the iterative process. Figure 14 shows the evolution of the normalized L2 norm of the cost functional gradient during the iterative process. Figure 15 shows the evolution of the global error during the minimization process.

The resolution of this test case has shown the importance of a good problem definition. A badly defined cost function can produce very strange final solutions, even if the process seems to converge very well.

Figures 13 and 14 show the convergence of the minimization process for case 3. The global error involved in the finite element computations has also been controlled

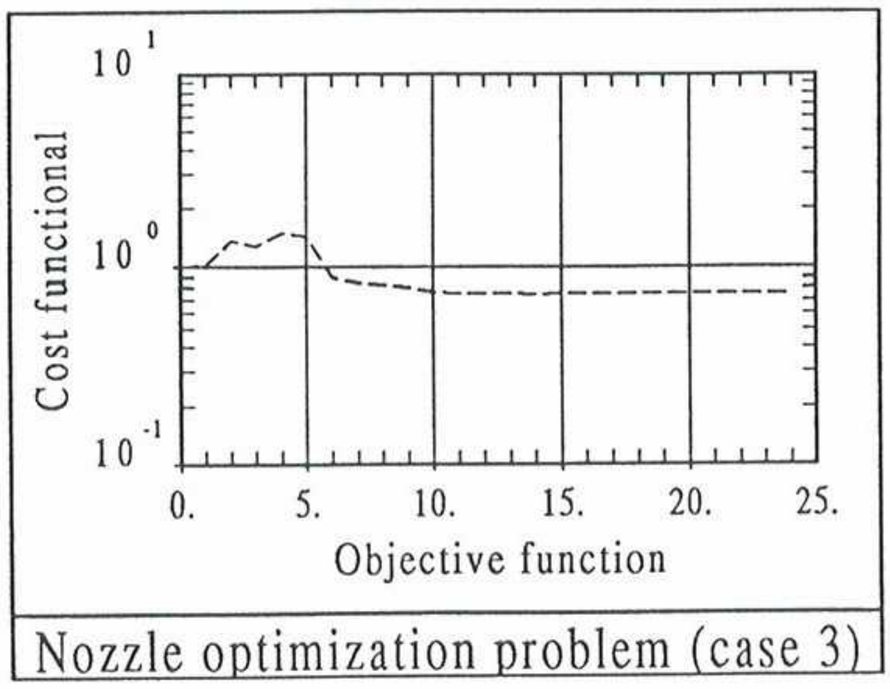

Figure 13. Evolution of the normalized cost functional.

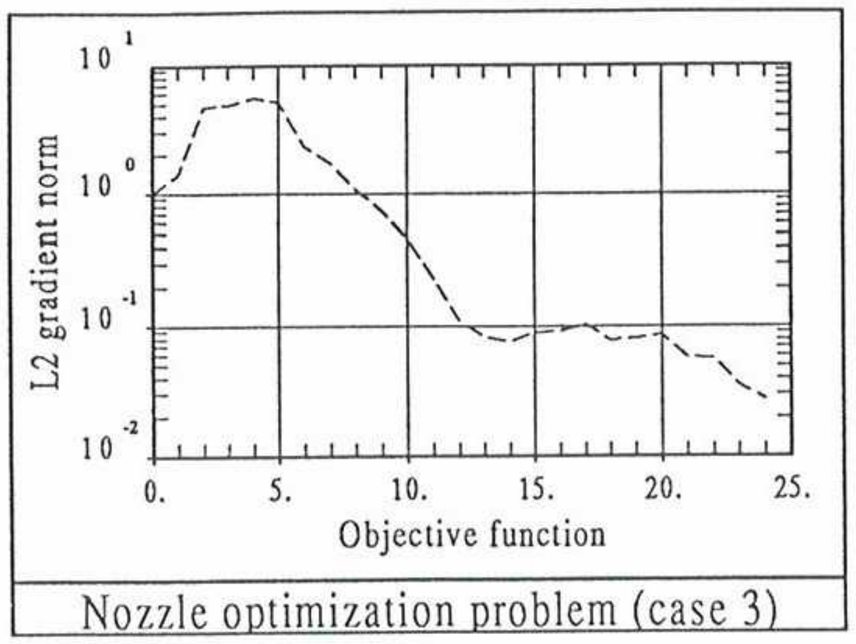

Figure 14. Evolution of the normalized L2 norm of the gradient of the cost functional.

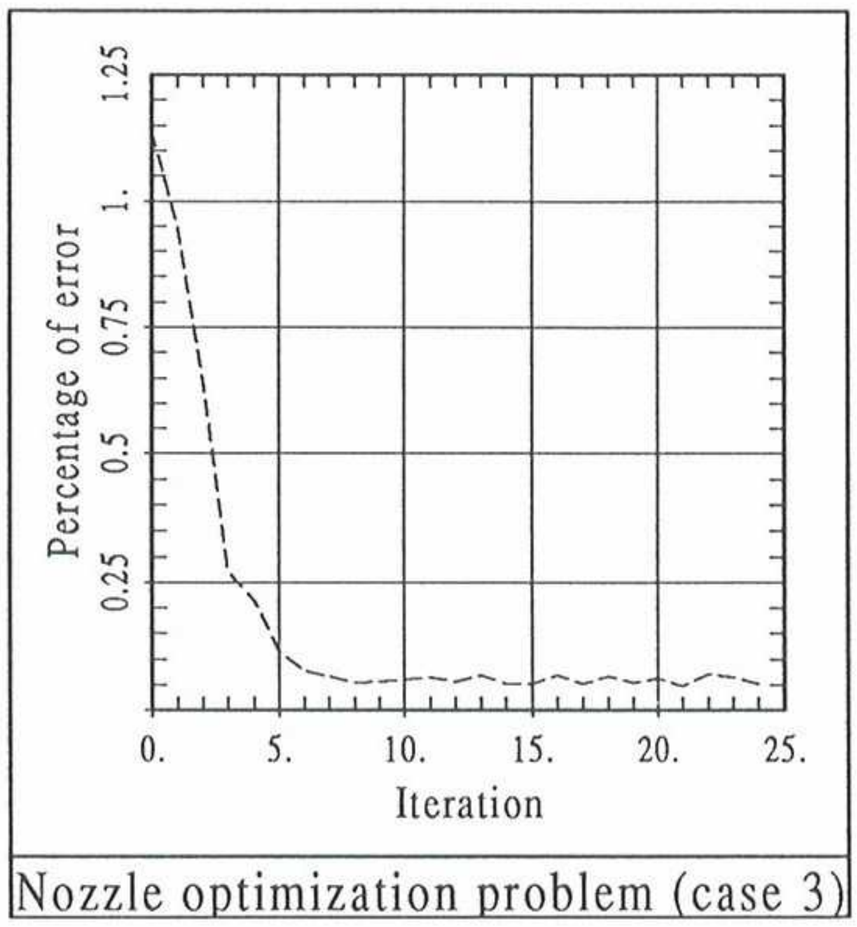

Figure 15. Evolution of the percentage of error.

and after the sixth iteration it has been kept below the 0.1% limit imposed at the beginning. Figure 12 shows a very satisfactory mesh for the final design.

9.3 T4 workshop test case

This test case consists in recovering the Korn airfoil at an angle of attack 0°. The target pressure coefficient C_p^{target} has been obtained by a direct computation of the Korn airfoil with a finite element code using the same methodology as in test case T1 (section 9.1) and a maximum global error of 0.1%. The infinite boundary is placed a distance of 10 chords from the profile. The initial design corresponds to a NACA 64A410 profile.

The inverse problem has been solved using a minimization approach. The cost functional to be minimized has been defined as:

$$f = \int_0^2 (C_p(x) - C_p^{target})^2 ds \tag{29}$$

This integral is extended around the profile and the integration variable is the arc s and not the x coordinate so that all the boundary is equally weighted. If the x variable is used the cost function tends to put more weight on the medium part of the profile and less on the edges.

The geometry of each design has been defined using 25 design variables. These variables are the y coordinates of 25 points distributed around the profile which are used to interpolate a B-spline. Figure 16 shows the initial shape and the finite element mesh used for the initial design. The 25 points used to define the shape of each design are all the nodes lying on the profile in Figure 16 with the exception of the trailing edge which is fixed. The maximum global error has been limited to 0.1% of the total potential norm.

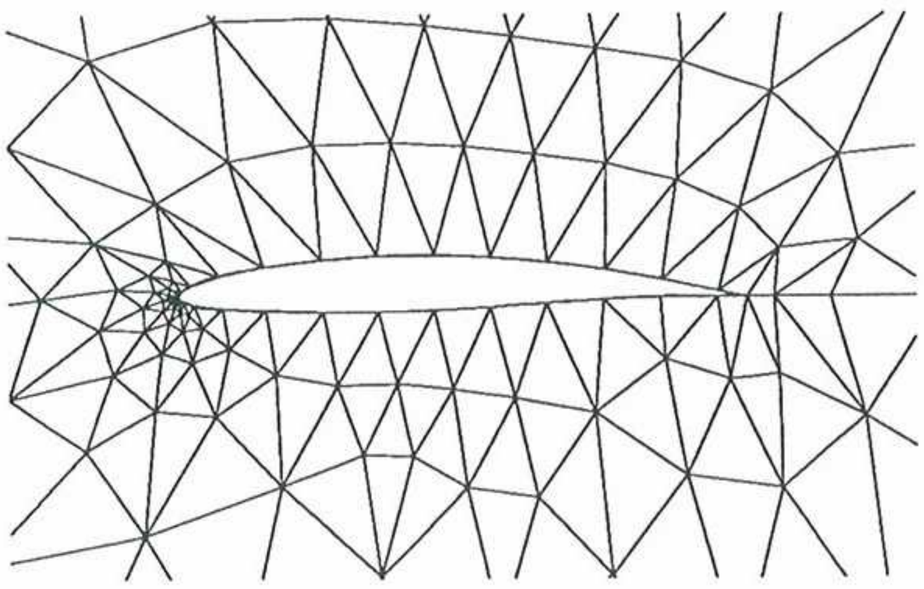

Figure 16. Initial shape, initial mesh and definition of the design variables.

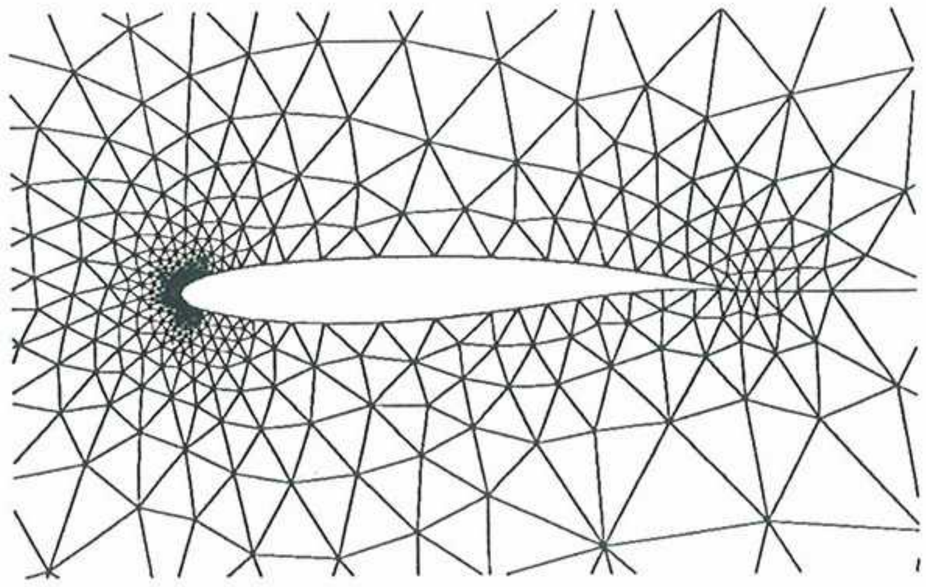

Figure 17. Final shape and final mesh.

The iterative process has converged after 50 iterations. The final shape and the final mesh can be observed in Figure 17. The whole problem has taken around 3.5 hours of CPU on a Silicon Graphics Indigo R4000 workstation.

The evolution of the normalized cost functional during the process can be seen in Figure 18. Figure 19 shows the evolution of the L2 difference norm between the solution profile and the design profile. This norm has been computed as the L2 difference norm between each design and the final one since no information on the exact definition of the Korn airfoil using the 25 control points was available. In fact it is not possible to define exactly the Korn airfoil using the 25 interpolating points. Figure 20 shows the evolution of the global error during the minimization process. The meshes used for the computations have around 2700 nodes and 1300 quadratic elements. Figure 21 shows the C_p distributions for the initial profile, the target profile and the last design obtained.

Figures 18 and 19 show a good convergence of the minimization process. The cost functional has been reduced almost 2 orders of magnitude in 50 iterations.

The global error involved in the finite element computations has been controlled. In fact it is very low compared with the 0.1% limitation. This is because the error is concentrated around the profile, but a little bit far away the flow is almost uniform and the error is almost null. This explains why the global error is small. The important

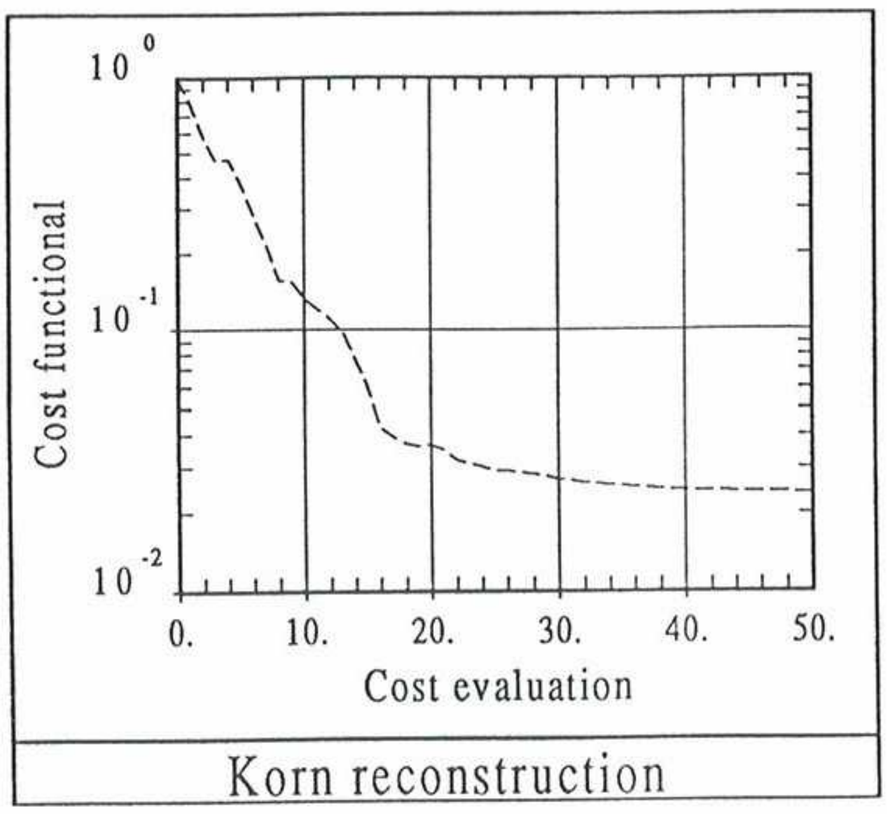

Figure 18. Evolution of the normalized cost functional during the iterative process.

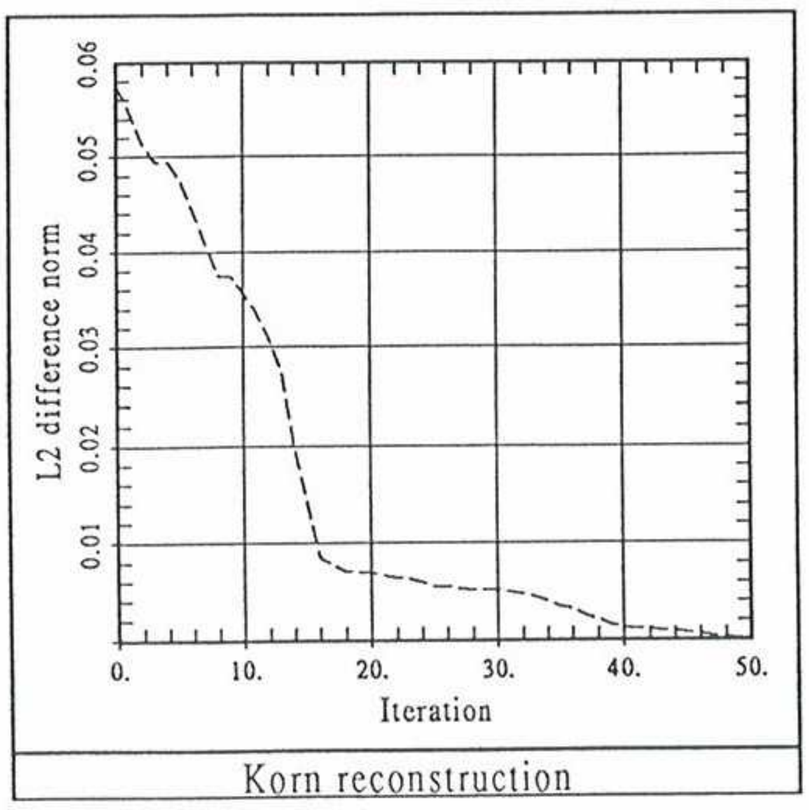

Figure 19. Evolution of the L2 difference norm between the solution profile and the design profile.

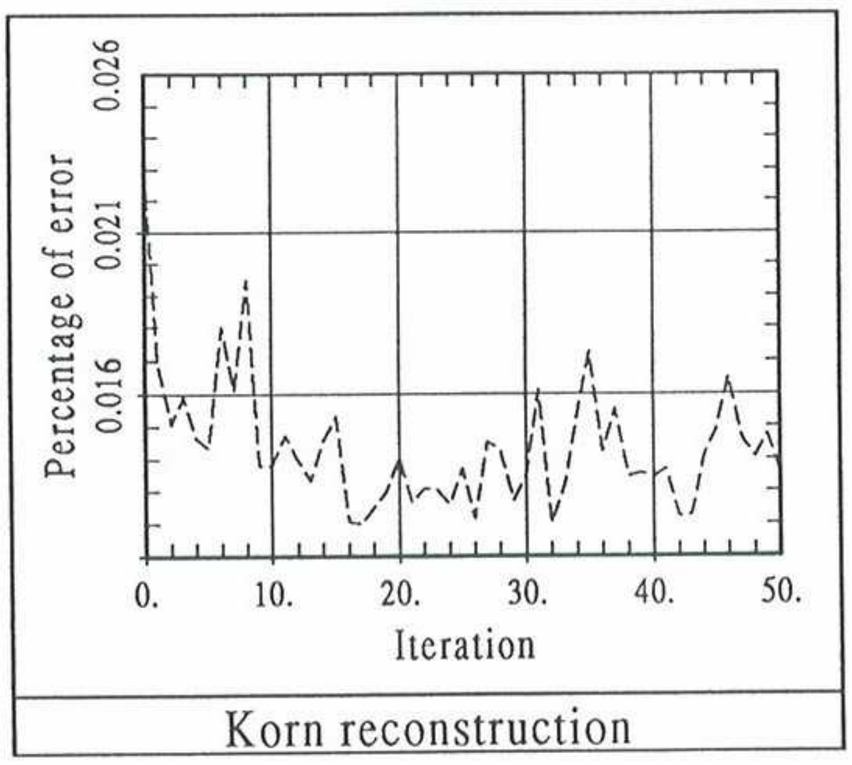

Figure 20. Evolution of the percentage of error.

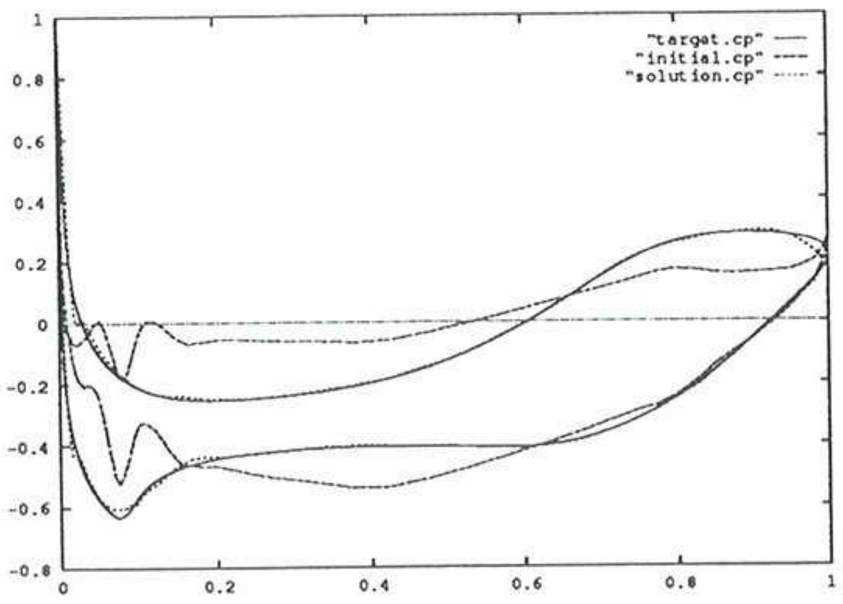

Figure 21. Distribution of C_p for the initial profile, the target design and the computed design.

issue, in fact, is how the error is distributed around the profile. Figure 17 shows how the mesh concentrates many more elements around the leading edge where the gradients of the potential are higher.

The comparison between the target and the computed C_p values shown in Figure 21 is quite good although some differences are still noticeable. On the other hand Figure 18 shows that the process seems to be converged, and it is not possible to get a solution closer to the target one. The reasons are that probably it is not possible to get a better definition of the Korn airfoil using a B-splines interpolation with 25 points. In fact the computations over the Korn airfoil have shown that it is extremely sensible to little changes in its shape. In order to get a better final solution it would be necessary to use more design variables to enhance the B-spline interpolation, but this would considerable increase the total cost.

The conclusions from this test case are:

- The methodology used works in a very satisfactory way producing a good final solution with an adequate final mesh.
- The convergence of the process can also be considered good.

- A study of the parametrization required to obtain a solution closer to the target one appears as very necessary.

9.4 Two elements inverse problem

In order to check the proposed methodology in cases with more than one airfoil a case with two elements have been studied. This case consists in recovering two NACA 0012 profiles at an angle of attack 0° positioned as shown in Figure 23. The starting design is formed by the two profiles as shown in Figure 22. Each profile has been obtained from a NACA 0012 reducing its thickness to one half and rotating each one 5° around their leading edges.

The target pressure coefficient C_p^{target} has been obtained by a direct computation of the target design as in the previous T4 test case.

The inverse problem has been solved using a minimization approach. The cost functional to be minimized has been defined as in eq. (29) extending the integral to the boundarys of both airfoils.

The geometry of each airfoil has been defined using 18 design variables. This variables are the y coordinates of 18 points distributed around each profile which are used to interpolate a B-spline. Figure 22 shows the initial shape and the finite element mesh used for the initial design. The 18 points used to define the shape of each profile are all the nodes lying on them in Figure 22 with the exception of the trailing and leading edges. For each profile, its rotation around its leading edge has been defined as an additional design variable. This means that two angles have been defined as design variables. The total number of design variables is thus 38. The maximum global error during the minimization process has been limited to a 0.2% of the total potential norm.

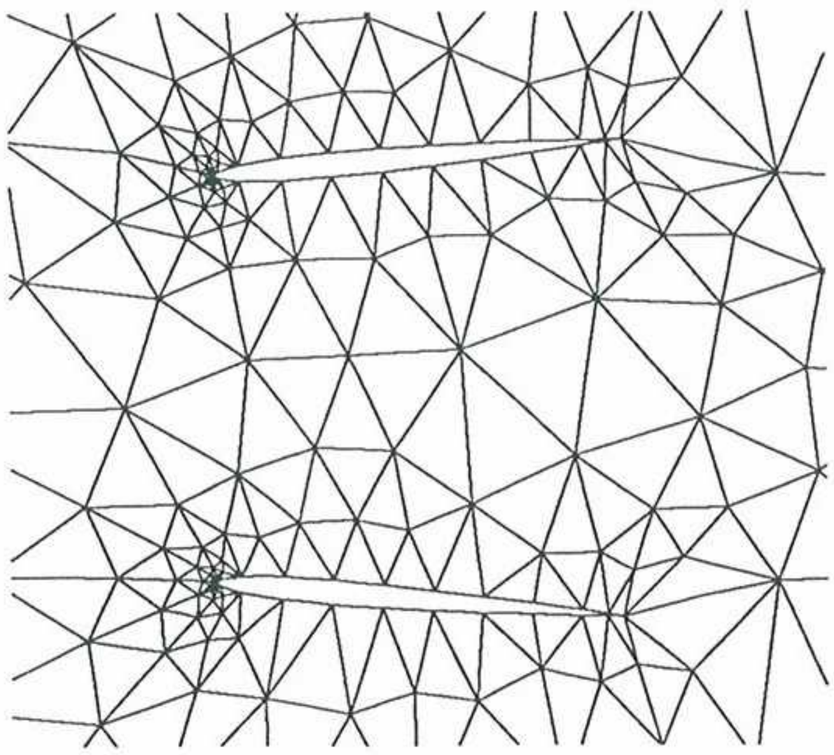

Figure 22. Initial shape, initial mesh and definition of the design variables.

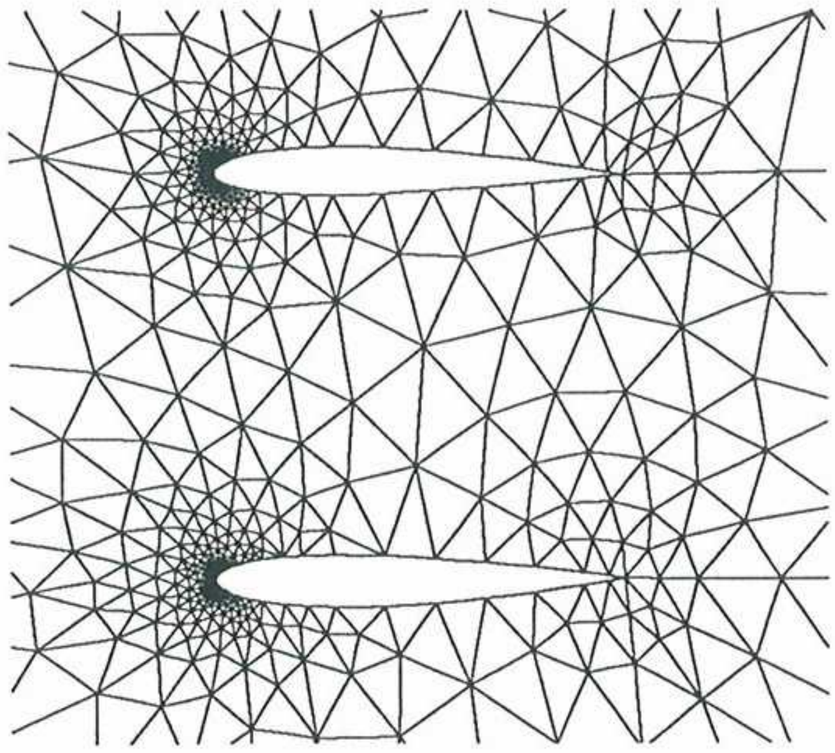

Figure 23. Final shape and final mesh.

The iterative process has been considered as converged after 100 iterations. The final shape and the final mesh can be observed in Figure 23. The whole problem has taken around 100 hours of CPU on a CONVEX C-3480 computer using 1 single processor. It is important to notice that the code has not been adapted to take advantage of the vectorial capabilities of the computer which could substantially reduce the computational cost.

The evolution of the normalized cost functional during the process can be seen in Figure 24. Figure 25 shows the evolution of the normalized L2 difference norm between the solution profile and the design profile. Figure 26 shows the evolution of the global error during the minimization process. The meshes used for the computations have around 2700 nodes and 1300 quadratic elements. Figures 27 and 28 show the superposition of the C_p distribution for the target profile and the last design for each airfoil.

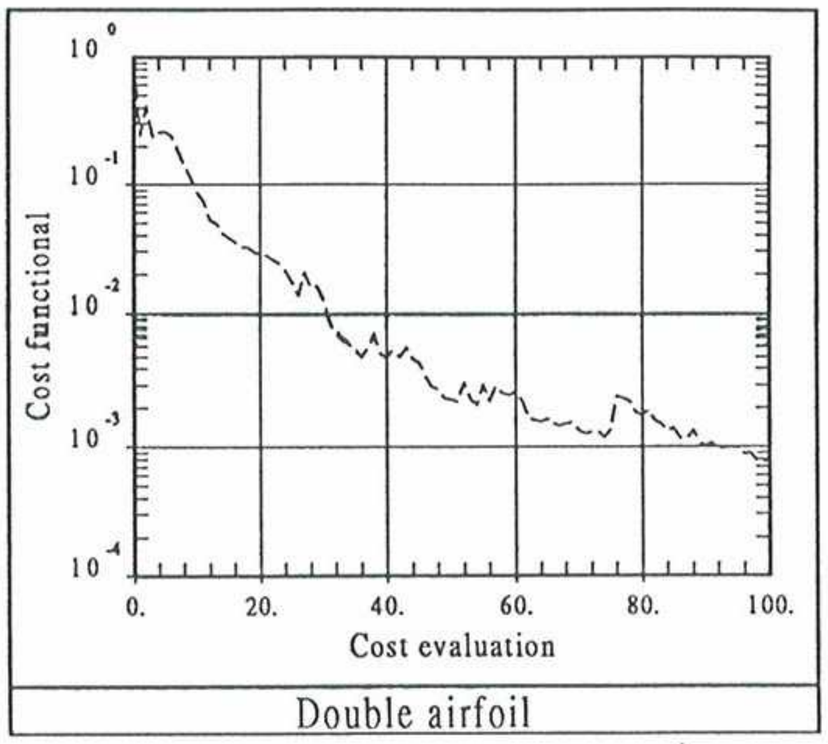

Figure 24. Evolution of the normalized cost functional during the iterative process.

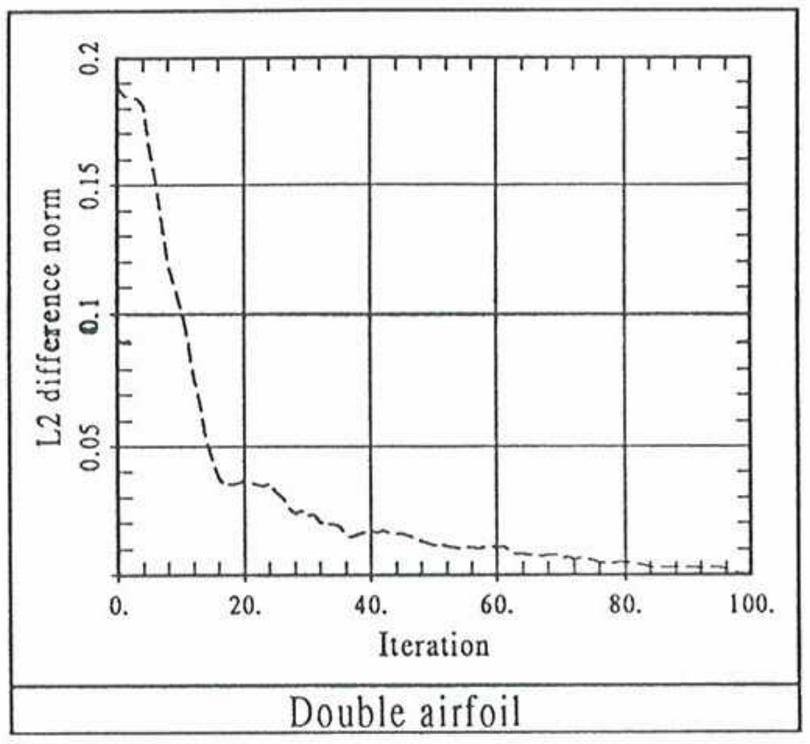

Figure 25. Evolution of the normalized L2 difference norm.

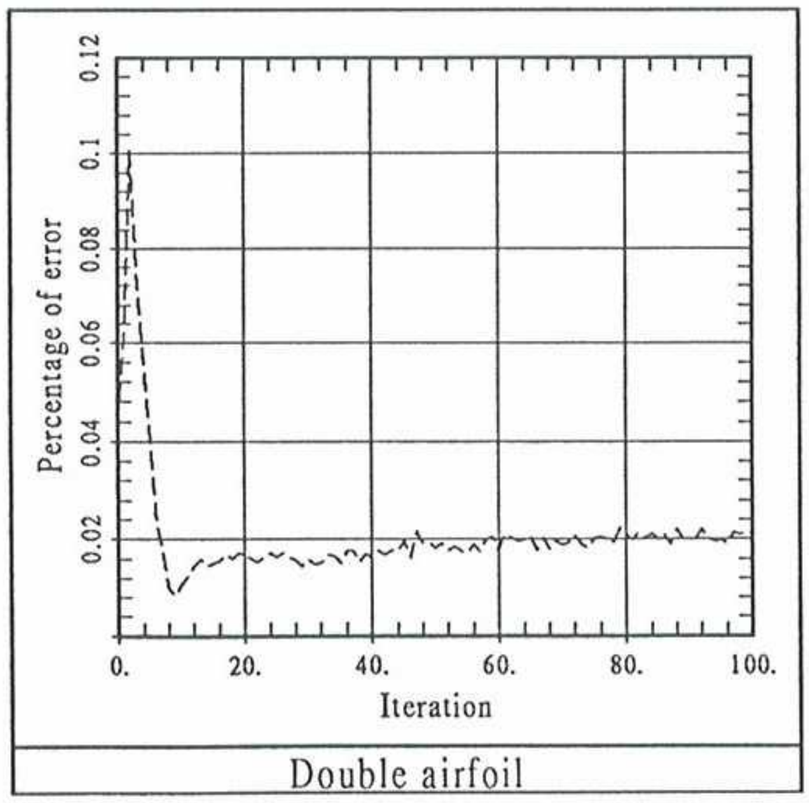

Figure 26. Evolution of the percentage of error.

Figures 24 and 25 show a good convergence of the minimization process. The cost functional has been diminished more than 3 orders of magnitude in 100 iterations.

The global error involved in the finite element computations has been completely controlled. In fact, as in the previous T4 test case, it is very low compared with the imposed limitation 0.2%.

The comparison between the target and the computed C_p shown in Figures 27 and 28 is quite good.

The same conclusions as in the previous T4 test case can be extracted. The key issue is the high CPU cost of the whole process. A big reduction of this cost is expected after vectorization of the code.

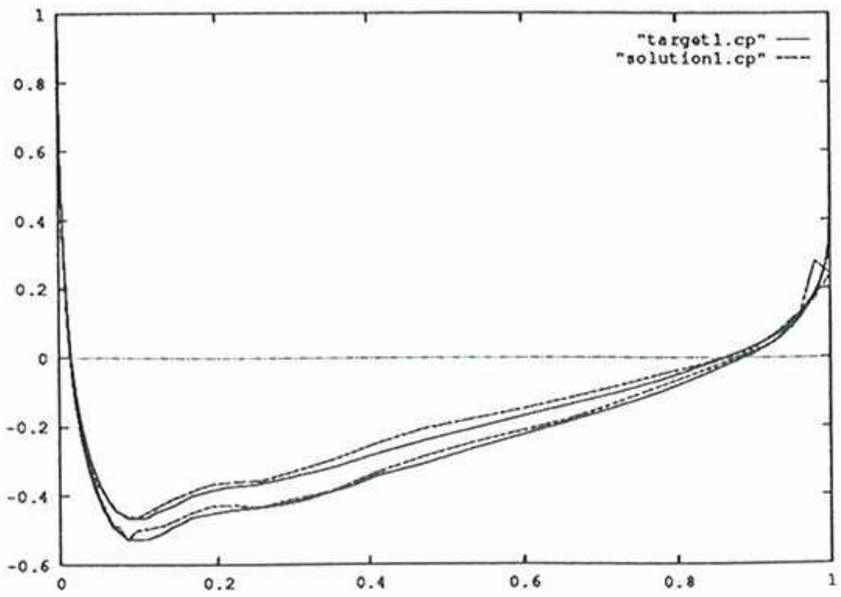

Figure 27. Distribution of C_p for the target and computed upper airfoils.

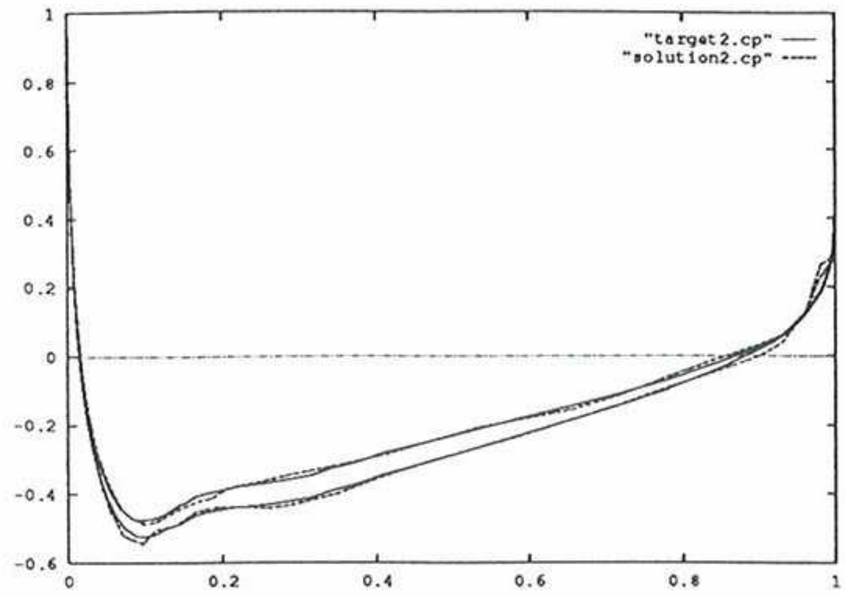

Figure 28. Distribution of C_p for the target and computed lower airfoils.

10. CONCLUSIONS

A new methodology for the resolution of optimization and inverse problems has been developed and assessed. This methodology is able to optimize the design and the analysis mesh together in order to produce a final design computed with a proper mesh.

Good quality results are obtained using a single mesh for each design without any remeshing. This considerably reduces the additional cost of the mesh control.

The presented methodology has provided excellent results for all the test cases analyzed leading to an accurate final solution with a good final mesh.

The use of a different "optimal" mesh for each design seems to be specially interesting to apply this methodology to more realistic flow models where the control of the mesh is crucial. This could be particularly attractive in presence of shocks.

11. ACKNOWLEDGMENTS

The authors acknowledge the support of the Commission of the European Communities DG-XII through the BRITE/EURAM project "Optimum Design in Aerodynamics".

12. REFERENCES

[1] Bugeda, G. "Utilización de técnicas de estimación de error y generación automática de mallas en procesos de optimización estructural." Ph. D. Thesis - Universitat Politècnica de Catalunya (1990) (In Spanish).

[2] Bugeda, G. and Oñate, E., "New adaptive techniques for structural problems", First European Conference on *Numerical Methods in Engineering*, Brussels, Belgium, September, 1992.

[3] Bugeda, G. and Oñate, E., "Adaptive mesh refinement techniques for aerodynamic problems", in *Numerical Methods in Engineering and Applied Sciences.* H. Alder, J. C. Heinrich, S. Lavanchy, E Oñate & B. Suárez (Eds.),

CIMNE-Barcelona 1992.

[4] Bugeda, G., Oñate, E., and Miquel, J. "Optimum Design in Aerodynamics" BRITE/EURAM AREA 5, Contract N° AERO-0026C, Proposal N° 1082. Mid-Term Report (1991).

[5] Bugeda, G., Oñate, E., and Miquel, J. "Optimum Design in Aerodynamics" BRITE/EURAM AREA 5, Contract N° AERO-0026C, Proposal N° 1082. Final Report (1992).

[6] Faux, I. D. and Pratt, M. J. "Computational Geometry for Design and Manufacture.", Edited by Ellis Horwood Limited, 1987.

[7] Navarrina, F. "Una metodología general para optimización estructural en diseño asistido por ordenador." Ph. D. Thesis - Universitat Politècnica de Catalunya (1987) (In Spanish).

[8] Navarrina, F., Bendito, E. and Casteleiro M. "High order sensitivity analysis in shape optimization problems." - *Computer Methods in Applied Mechanics and Engineering, vol. 75, pp. 267-281 (1989)*

[9] Oñate, E., Castro, J. and Kreiner, R., "Error estimations and mesh adaptivity techniques for plate and shell problems", presented at the *3rd. International Conference on Quality Assurance and Standards in Finite Element Methods*, Stratford-upon-Avon, England, 10–12 September, 1991.

[10] Oñate, E. and Castro, J., "Adaptive mesh refinement techniques for structural problems", published in *"The Finite Element Method in the 90's. A book dedicated to O. C. Zienkiewicz"*, E. Oñate, J. Periaux and J. Samuelsson (Eds.), Springer-Verlag&CIMNE, Barcelona 1991.

[11] Oñate, E. and Bugeda, G., "A Study of Mesh Optimality Criteria in Adaptive Finite Element Analysis" to be published in *"Engineering Computations"*

[12] Peraire, J. "A Finite Element Method for Convection Dominated Flows." - Ph. D. Thesis - University College of Swansea (1986)

[13] Peraire, J., Morgan, K. and Peiró, J. "Unstructured finite element mesh generation and adaptive procedures for CFD." - *AGARD FDP: Specialist's Meeting, Loen, Norway (1989)*

[14] Pironneau, O. "Méthodes des éléments finis pour les fluides." Masson 1988.

[15] Zienkiewicz, O.C. and Zhu, J.Z., "A simple error estimator and adaptive procedure for practical engineering analysis", *Int. Num. Meth. Engrg.*, **24**, 337–357, 1987.

[16] Zienkiewicz, O.C., Zhu, J.Z., Liu, I.C., Morgan, K. and Peraire, J., "Error estimates and adaptivity from elasticity to high speed compressible flow", in J.R. Whiteman, ed., MAFELAP 87, 483–512, Academic Press, New York, 1988.

[17] Zhu, J.Z. and Zienkiewicz, O.C., "Adaptive techniques in the finite element method", *Comm. Appl. Numer. Methods*, **4**, 197–204, 1988.

[18] Zienkiewicz, O.C., Zhu, J.Z. and Gong, N.G., "Effective and practical $h-p$ version adaptive analysis procedures for the finite element method", *Internat. J. Numer. Methods Engrg.*, **28**, 879–891, 1989.

[19] Zienkiewicz, O.C., Zhu, J.Z., "The three R's of engineering analysis and error estimation and adaptivity", *Comp. Meth. in Appl. Mech. and Engng*, **82**, 95-113, 1990.

[20] Brite Euram 1082 partners, "Workshop on Selected Inverse and Optimum Design Problems. Definition of Test Cases" (1992).